JOURNAL OF FORENSIC SCIENCES

J Forensic Sci, March 2016, Vol. 61, No. 2
doi: 10.1111/1556-4029.13017
Available online at: onlinelibrary.wiley.com

TECHNICAL NOTE

DIGITAL & MULTIMEDIA SCIENCES

Hui Zeng,[1] *Ph.D.; and Xiangui Kang,*[1] *Ph.D.*

Fast Source Camera Identification Using Content Adaptive Guided Image Filter*

ABSTRACT: Source camera identification (SCI) is an important topic in image forensics. One of the most effective fingerprints for linking an image to its source camera is the sensor pattern noise, which is estimated as the difference between the content and its denoised version. It is widely believed that the performance of the sensor-based SCI heavily relies on the denoising filter used. This study proposes a novel sensor-based SCI method using content adaptive guided image filter (CAGIF). Thanks to the low complexity nature of the CAGIF, the proposed method is much faster than the state-of-the-art methods, which is a big advantage considering the potential real-time application of SCI. Despite the advantage of speed, experimental results also show that the proposed method can achieve comparable or better performance than the state-of-the-art methods in terms of accuracy.

KEYWORDS: forensic science, image forensics, source camera identification, sensor pattern noise, denoising filter, content adaptive guided image filter

The origin information of a digital image or video is important in forensic research area as well as in applications; for example in law enforcement, the investigator would be interested in linking images of illegal content to a certain camera. One of the most effective fingerprints for linking an image to its source camera is the sensor pattern noise (SPN) (1), which is caused by photo-response nonuniformity (PRNU) due to inhomogeneity of silicon wafers (2). An important advantage of SPN is that it can identify not only camera models, but also individual cameras of the same model (3).

In the most widely accepted sensor-based source camera identification (SCI) method (3), SPN is estimated as the difference between the content and its wavelet denoised version (4), and its correlation to the fingerprint of a given camera is used to measure the probability that an image originated from that camera. Owing to its wide applications in source identification and integrity verification, this method has been fully studied and various enhancements have emerged recently. Existing enhancements to SCI are classifiable in three categories:

1 Better filters are adopted in extracting SPN from the image (5,6).
2 Better strategies or metrics are adopted to measure the correlation between the SPN from an image and the fingerprint of a reference camera (7–10).
3 Postprocessing the extracted SPN to further suppress the unwanted artifacts, for example color interpolation, row and column artifacts, and contamination of the image details (7,11).

Our research lies in the first category enhancement of SCI. Unlike other state-of-the-art SCI methods, in this method, SPN is extracted from an image using a content adaptive guided image filter (CAGIF) (12). Thanks to the low complexity nature of CAGIF, the proposed method is much faster than other the state-of-the-art methods, which is a big advantage considering the potential real-time application of SCI. Despite the advantage of speed, experimental results also show that the proposed method achieves comparable or better performance than the state-of-the-art SCI methods in terms of accuracy. In this study, boldface symbols represent either vectors or matrices.

The rest of the paper is organized as follows. In the next section, we briefly review of the process of sensor-based SCI and the denoising filters used in the state-of-the-art literatures. The third section introduces CAGIF and the proposed CAGIF-based SCI method. The fourth section shows the experimental results. The proposed method is compared with other methods in terms of both accuracy and speed. The conclusion is given in last section.

Brief Review of Source Camera Identification

In this section, we briefly explain the SCI method developed in ref. (3) and some improved algorithms that relate most to our work.

The PRNU of the imaging sensor is usually modeled as a multiplicative factor that is unique to a camera A. Taking the PRNU factor $\boldsymbol{K}_{\mathrm{A}}$ into consideration, the raw camera output $\boldsymbol{I}$ can be written as:

$$\boldsymbol{I} = \boldsymbol{I}_0(1 + \boldsymbol{K}_A) + \boldsymbol{\theta} \tag{1}$$

where $\boldsymbol{I}_0$ is the noise-free image, and $\boldsymbol{\theta}$ refers to other noise elements which usually believed to be zero-mean.

[1]School of Information Science & Tech., Sun Yat-sen University, Guangzhou 510006, China.

*Supported by NSFC (Grant Nos 61379155 and U1135001), 973 Program (Grant No. 2011CB302204), the Research Fund for the Doctoral Program of Higher Education of China (Grant No. 20110171110042), and NSF of Guangdong Province (Grant No. 2013020012788).

Received 28 Jan. 2015; and in revised form 9 June 2015; accepted 27 June 2015.

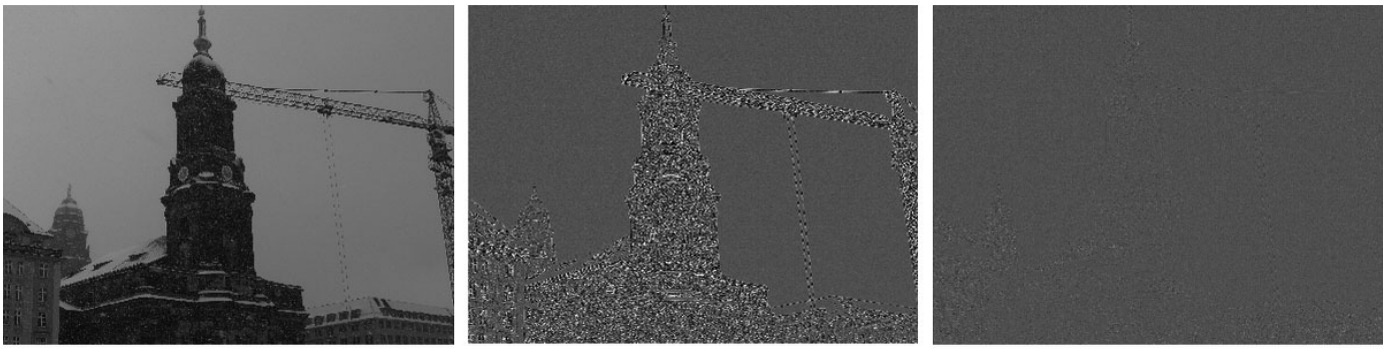

FIG. 1—*Comparison of extracted SPN with different filters. (a) the image, (b) extracted SPN with GIF (16), and (c) extracted SPN with CAGIF (12). For display purpose, the SPNs are scaled to [−0.1, 0.1]. SPN, sensor pattern noise; CAGIF, content adaptive guided image filter.*

In the SCI, the SPN $\boldsymbol{W}$ of a given image can be roughly estimated as the difference between itself and its denoised version.

$$\boldsymbol{W} = \boldsymbol{I} - F(\boldsymbol{I}) \tag{2}$$

where F is the used denoising filter. The fingerprint $\boldsymbol{K}$ of a given camera can then be estimated from a number of images from this camera with a maximum likelihood approach (7):

$$\boldsymbol{K} = \frac{\sum_{i=1}^{N} \boldsymbol{W}^{(i)} \boldsymbol{I}^{(i)}}{\sum_{i=1}^{N} (\boldsymbol{I}^{(i)})^2} \tag{3}$$

where N is the number of images used to estimate $\boldsymbol{K}$. A correlation statistic is used to measure the similarity between the $\boldsymbol{W}$ and $\boldsymbol{IK}$, such as peak-to-correlation-energy (PCE) value (8), which is defined as:

$$\mathrm{PCE} = \frac{\boldsymbol{\rho}_{(0,0)}^2}{(1/(|s| - |\boldsymbol{\Omega}|)) \sum_{s \notin \boldsymbol{\Omega}} \boldsymbol{\rho}_s^2} \cdot \mathrm{sign}(\boldsymbol{\rho}_{(0,0)}) \tag{4}$$

where $\boldsymbol{\rho}$ is the normalized cross-correlation between $\boldsymbol{W}$ and $\boldsymbol{IK}$, and s is the map of all entries of $\boldsymbol{\rho}$. $\boldsymbol{\Omega}$ represents a small region around $\boldsymbol{\rho}_{(0,0)}$and $|\boldsymbol{\Omega}|$ is the number of entries in $\boldsymbol{\Omega}$. The greater the PCE value is, the higher the probability that the test image is taken by the reference camera. In the following, such wavelet-based SCI method is denoted as *wavelet* method for short.

Owing to the imperfection of F, the extracted SPN $\boldsymbol{W}$ contains not only a desired $\boldsymbol{K}_A$-dependent part, but also an undesired image content-dependent part, which can be seen from Fig. 1. Generally speaking, the SCI results is less reliable when more content-dependent residue remain in $\boldsymbol{W}$.

To enhance the performance of SCI, some researchers have tried several filters for denoising. In ref. (5), the sophisticated BM3D filter (13) is introduced to extract SPN from an image. BM3D, which builds on the concept of nonlocal means by identifying similar patches in an image and groups them together, has proved to be very effective in image denoising. However, the searching and grouping process is time-consuming. Moreover, BM3D is a nonblind denoising algorithm that needs the noise level parameter provided when used for SCI purpose. Different parameter settings cause the inconsistency in the reported results (5,10,14). In the following, such SCI method is denoted as the *BM3D* method. In ref. (6), anisotropic diffusion (15) is used to extract SPN from an image. The authors in ref. (6) applied a median filter followed by an anisotropic diffusion filter to get the denoised image. It is reported that the computation complexity of such method is lower than that of *wavelet* method. However, this method includes a sorting step to determine a constant that controls the diffusion (see refs [6] or [15] for detail), which is time-consuming when filtering a high-resolution image. Such anisotropic diffusion-based SCI method is denoted as the *Anisotropic* method in the following.

Methods

In this section, we first briefly review the newly developed CAGIF, and then give detail about the proposed CAGIF-based SCI method.

Content Adaptive Guided Image Filtering

Guide image filtering (GIF) is one of the most successful local filtering in recent years (16).[a] Compared with the global optimization filters, GIF is much simpler and faster while performing well in multiple applications, for example, image smoothing/enhancement, denoising, and dehazing. The output image $\hat{\boldsymbol{I}}$ of the GIF is locally computed as a linear transform of the guidance image $\boldsymbol{G}$ which can be the input image $\boldsymbol{I}$ or another image.

$$\hat{\boldsymbol{I}}_p = \frac{1}{|w|} \left(\sum_{k \in w_p} a_k \boldsymbol{G}_p + b_k \right) \tag{5}$$

where w_p is a square window centered at pixel p of a radius r, and the coefficients a_k and b_k are determined using linear regression

$$\begin{aligned} a_k &= \frac{(1/|w|) \sum_{p \in w_k} \boldsymbol{G}_p \boldsymbol{I}_p - \bar{\boldsymbol{G}}_k \bar{\boldsymbol{I}}_k}{\sigma_k^2 + \varepsilon} \\ b_k &= \bar{\boldsymbol{I}}_k - a_k \bar{\boldsymbol{G}}_k \end{aligned} \tag{6}$$

where $\bar{\boldsymbol{G}}_k$ and $\bar{\boldsymbol{I}}_k$ denote the mean values of $\boldsymbol{G}$ and $\boldsymbol{I}$ in window w_k, and σ_k^2 is the variance of $\boldsymbol{G}$ in w_k. ε is a predefined smoothing parameter adjusting the smooth degree of $\hat{\boldsymbol{I}}$.

[a]GIF has been included in Matlab2014 as a function *imguidedfilter*().

The edge-preserving nature of GIF can be explained as following. Consider the case that $\boldsymbol{I} = \boldsymbol{G}$. In the weak textural area, $a_k \approx 0$ and $b_k \approx \bar{\boldsymbol{I}}_k$, GIF reduced to a mean filter. In the high textural area, $a_k \approx 1$, $b_k \approx 0$ and $\hat{\boldsymbol{I}}_p \approx \boldsymbol{I}_p$; that is, its value unchanged.

Despite its excellent performance, GIF shares a common limitation of other local filters – it may have halos near some edges. These halo artifacts are undesired when used to extract SPN for SCI purpose, which can be observed from Fig. 1. Hence, we adopt a refined version of GIF, which is called CAGIF (12). CAGIF that incorporates edge aware weighting into GIF can prevent halo artifacts while preserving the advantages of fast and simple. In CAGIF, an edge aware weighting is computed as

$$\boldsymbol{\Gamma}_k = \frac{1}{N}\sum_{p=1}^{N} \frac{\left(\left(\sigma_k^2 + v_1\right)/\left(\bar{\boldsymbol{G}}_k^2 + 10^{-9}\right)\right)^{0.75}}{\left(\left(\sigma_p^2 + v_1\right)/\left(\bar{\boldsymbol{G}}_p^2 + 10^{-9}\right)\right)^{0.75}} \tag{7}$$

where N is the total number of pixels in $\boldsymbol{G}$, and υ_1 is $(0.001*L)^2$ with L being the dynamic range of $\boldsymbol{G}$. Owing to the box filter in ref. (16), the complexity of $\boldsymbol{\Gamma}_k$ is $O(N)$. After $\boldsymbol{\Gamma}_k$ is obtained, the smoothing parameter ε in Eq. (6) is adjusted as $\boldsymbol{\Gamma}_k$. The idea behind such modification is adopting larger ε in weak textural area and small ε for the pixel at an edge. CAGIF preserves edges better than GIF, so the SPN extracted by CAGIF contains less content-dependent residue than that extracted by GIF as shown in Fig. 1. Figure 1(*b*) shows the extracted SPN from Fig. 1(*a*) when GIF is used as the denoising function F. Figure 1(*c*) shows the extracted SPN from Fig. 1(*a*) with CAGIF, from which it is observed that the content-dependent residue has been significantly suppressed.

SPN Extraction with CAGIF

As discussed in previous subsection, CAGIF is more effective in extracting SPN compared with GIF. However, we experimentally find that the content-dependent residue after CAGIF is still relatively strong for strong textured images. The experiments in ref. (16) suggest a small radius r if more detail needs to be preserved in the filtered image (which means less content-dependent residue in SPN). Hence, we adopt a flexible strategy in determining the radius r of CAGIF according to the textural strength.

To measure the textural strength of a given image, we adopt the normalized total variation (TV) metrics (17), which is defined as the Dll_1 norm of the first-order derivatives divided by the size of the image. It should be pointed out that any other metrics which can measure the textural strength of a given image can be used here. TV is adopted in this study mainly for speed consideration. The histogram of TV for all the 2000 images involved in this study is shown in Fig. 2. It is observed that the TV values of most images are below 36 (more than 99% according to the experiment). Hence, the radius r is determined according to following strategy.

$$r = \begin{cases} 6 - \text{round}\,(\text{TV}/8) & \text{TV} < 36 \\ 2 & \text{otherwise} \end{cases} \tag{8}$$

The idea behind this strategy is quite intuitive: larger r for smoother images and small r for textural images. To further eliminate the impact of content-dependent residue, the range of the extracted SPN value is limited to $[-T, T]$ by truncating the out of range values to $-T$ or T. The final obtained SPN $\boldsymbol{W}$ can be denoted as

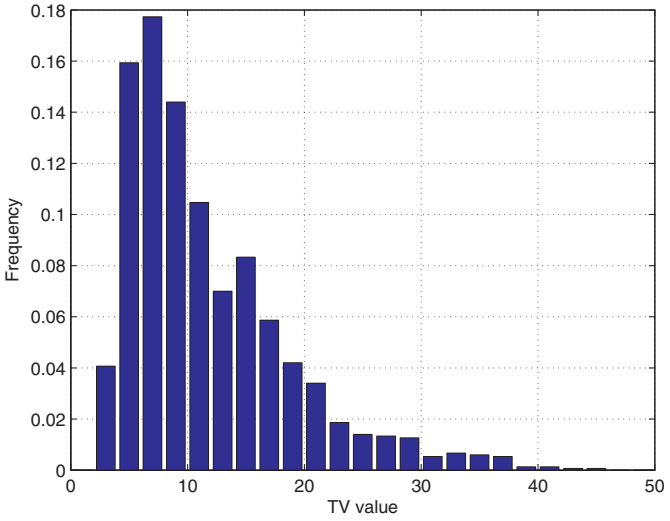

FIG. 2—*Histogram of TV values for 2000 high-resolution images of various indoor and outdoor scenes.*

$$\boldsymbol{W} = \text{truncate}_T[\boldsymbol{I} - \text{CAGIF}_\varepsilon(\boldsymbol{I})] \tag{9}$$

where $\text{CAGIF}_\varepsilon(\cdot)$ denotes CAGIF with smoothing parameter ε. The experiment shows that the final SCI performance is insensitive with T in a large range ($T \in [5, 10]$), and we set $T = 6$ in this study.

Once the SPN $\boldsymbol{W}$ from a single image is obtained, the fingerprint $\boldsymbol{K}$ of a given camera is estimated from a number of images in the same way of Eq. (3).

Results and Discussion

This section compares the proposed method with three other the state-of-the-art SCI methods, for example *wavelet* method (8), *BM3D* method (5) and *Anisotropic* method (6).

Experimental Setup

The data set is composed of 1500 images from six cameras of the Dresden Image Database (18), and 500 images from two cameras of our own database, each camera responsible for 250 images. Table 1 shows the camera model, image format and original resolution. Note we intentionally choose cameras with the same or similar model, which is believed to be more challenging for SCI.

For each camera, 50 images are used to estimate fingerprint $\boldsymbol{K}$ and the remaining 200 images are used for test. To reduce the influence of the camera models to the final SCI performance, the

TABLE 1—*Images used in the experiments.*

Camera	Original Resolution	Format
Panasonic DMC-FZ50 C0	3648 × 2736	JPEG
Panasonic DMC-FZ50 C1	3648 × 2736	JPEG
Kodak M1063 C0	3664 × 2748	JPEG
Kodak M1063 C1	3664 × 2748	JPEG
Nikon D200 C0	3872 × 2592	JPEG
Nikon D200 C1	3872 × 2592	JPEG
Canon PS A610	2592 × 1944	JPEG
Canon PS A620	3072 × 2304	JPEG

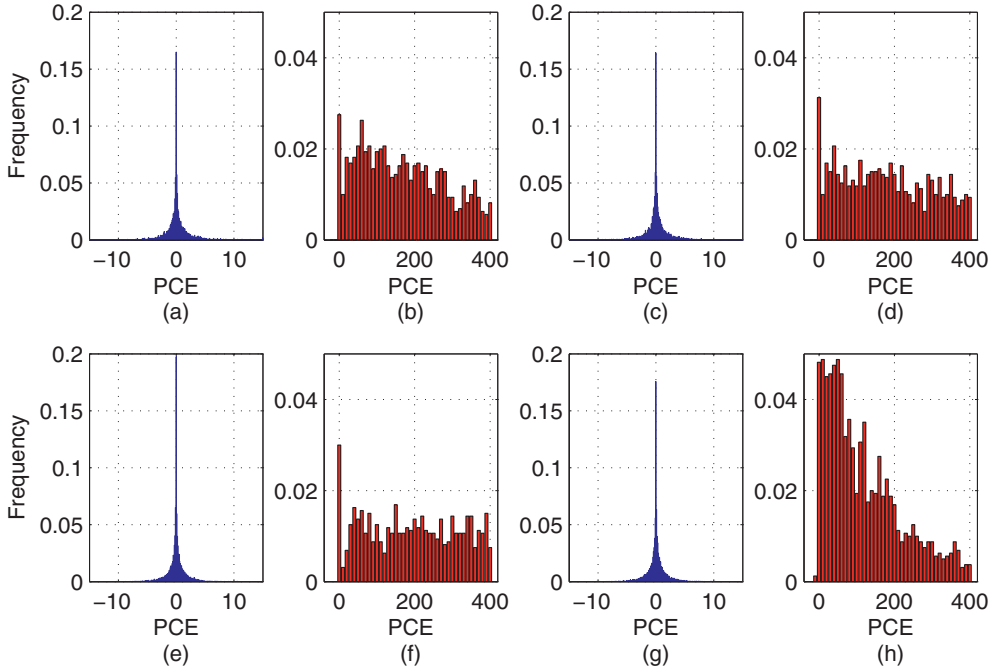

FIG. 3—*Histogram of PCE for small-size images. (a, b) negative samples and positive samples with CAGIF, (c, d) negative samples and positive samples with wavelet (8), (e, f) negative samples and positive samples with BM3D (5), (g, h) negative samples and positive samples with Anisotropic (6). For display purpose, the histogram of PCE >400 is omitted for positive samples. CAGIF, content adaptive guided image filter; PCE, peak-to-correlation-energy.*

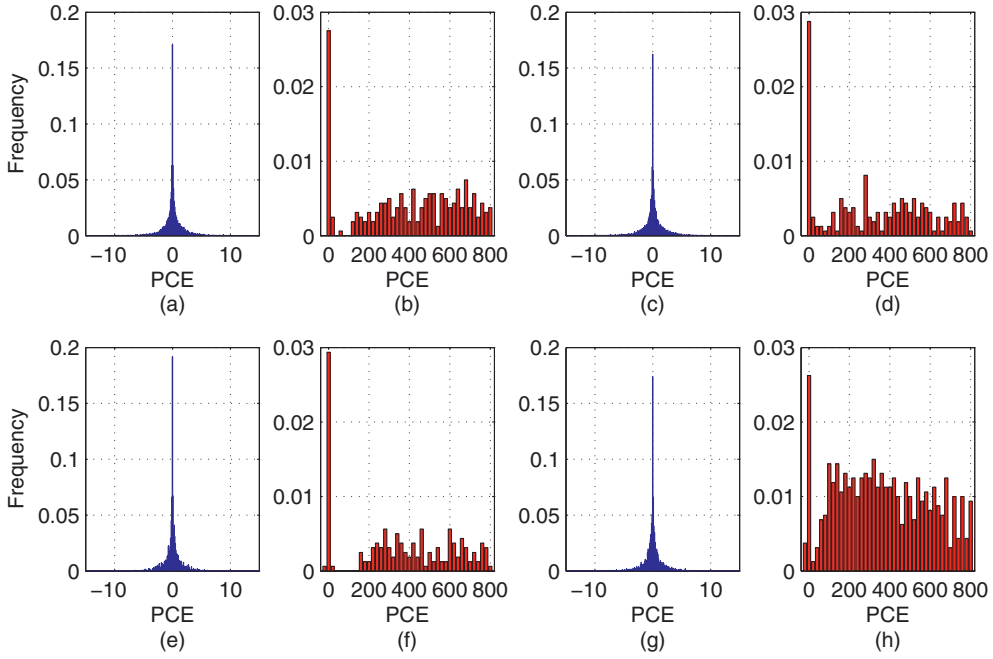

FIG. 4—*Histogram of PCE for original-size images. (a, b) negative samples and positive samples with CAGIF, (c, d) negative samples and positive samples with wavelet (8), (e, f) negative samples and positive samples with BM3D (5), (g, h) negative samples and positive samples with Anisotropic (6). For display purpose, the histogram of PCE >800 is omitted for positive samples. CAGIF, content adaptive guided image filter; PCE, peak-to-correlation-energy.*

SCI results of all cameras are synthesized in this study; that is, for each of the following tests, we have $8 \times 200 = 1600$ positive samples and $8 \times (8–1) \times 200 = 11200$ negative samples. Two image sizes are tested in this study; the one is *original* size, where the smallest original resolution in the database (2592×1944) is used, the other is *small* size, where all images are cropped from the center to the size of 1024×768. For fair comparison, extracted SPNs with all methods are postprocessed as that in ref. (7) to suppress the unwanted artifacts, for example color interpolation, row and column artifacts. For the CAGIF method, smoothing parameter ε is set as 0.02. For the *BM3D* method, we set the required parameter $\sigma = 5$ as recommended in ref. (14). The experiments show that this setting is near optimal for SCI purpose.

Performance Comparison

Figure 3 shows the histogram of the PCE values of the *small*-size images with the proposed CAGIF method, *wavelet* method, *BM3D* method and *Anisotropic* method, respectively. For all of the four SCI methods, PCE values of the most negative samples are below 15. Hence, the number of positive samples whose PCE value below 15 (the first two bars of positive samples in Fig. 3) is critical for classification. To highlight the distribution of small PCE part, the histogram of PCE >400 is omitted for the positive samples in Fig. 3. By examining the probability that PCE value of positive samples below 15, it is observed that the *BM3D* method and the CAGIF method perform best among the four SCI methods. Figure 4 shows the histogram of the PCE values on the *original*-size images with different SCI methods. The histogram of PCE >800 for the positive samples is omitted. It is observed that the CAGIF method performs best among the four SCI methods in this case.

The ROC curves are shown in Fig. 5 to give a more direct comparison among the four SCI methods. *x*-axis is the false-positive rate calculated by the number of false acceptance images over the total number of negative samples. *y*-axis is the true positive rate calculated by the number of true acceptance images over the total number of positive samples. It is observed that the proposed CAGIF method achieves best performance in most cases among the four SCI methods. For example, for the *small*-size images, if the false-positive rate is fixed as 0.02, the true positive rates of the four SCI methods are 0.971, 0.969, 0.97 and 0.953, respectively. For the *original*-size images, if the false-positive rate is fixed as 0.02, the true positive rates of the four SCI methods are 0.989, 0.984, 0.978 and 0.97, respectively.

Robustness to JPEG Compression

Most images on the internet are further JPEG compressed for speed and storage consideration, and it is widely believed that the SPN becomes weak if the image is JPEG compressed. To

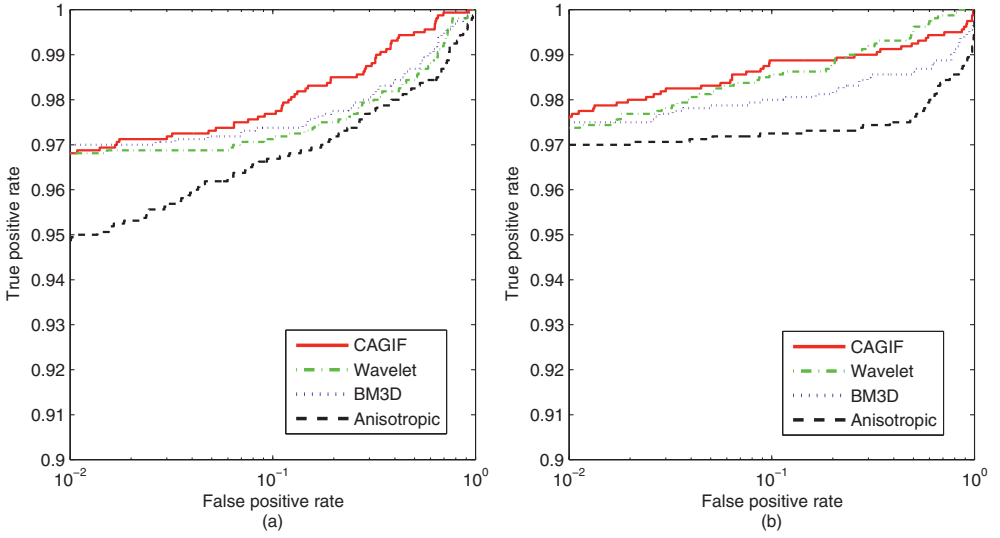

FIG. 5—*Performance comparison in terms of ROC curves. (a) small size (1024 × 768), (b) original size (2592 × 1944).*

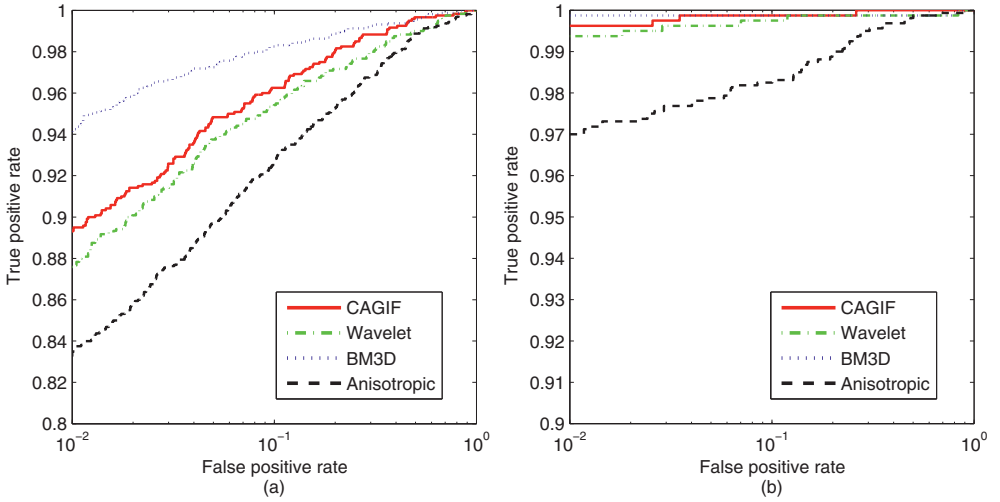

FIG. 6—*ROC curves for JPEG compressed images, quality factor (QF) = 75. (a) small size (1024 × 768), (b) original size (2592 × 1944).*

TABLE 2—*Time comparison (s) of extracting SPN from a test image.*

Method	Running Time for a *Small* Size Image	Running Time for an *Original* Size Image
Ours	0.42	2.9
Wavelet (8)	1.5	13
BM3D (5)	10.1	43
Anisotropic (6)	2.7	19

TABLE 3—*Time comparison (s) of extracting SPN from a test image on GPU.*

Method	Running Time for a *Small* Size Image	Running Time for an *Original* Size Image
Ours	0.15	0.71
Wavelet (8)	0.68	1.78
Anisotropic (6)	0.82	4.65

examine the robustness of the SCI method to JPEG compression, the test images in this subsection are JPEG compressed with quality factor (QF) 75. Fingerprint $\boldsymbol{K}$ of cameras are the same as that used in previous subsection.

The ROC curves of the four methods are shown in Fig. 6. It is observed that all of the four SCI methods are robust to JPEG compression despite some decline in ROC performance. The *BM3D* method performs best among the four SCI methods and the CAGIF method ranks second. It is interesting to find that the SCI performance on *original*-size images after JPEG compression is better than that before JPEG compression. This is because some positive samples before JPEG compression show a negative PCE value in the SCI test, which can be observed from the leftmost bins of Fig. 4. Such phenomenon rarely occurs after JPEG compression.

Computation and Efficiency

To extract SPN from an image with N pixels with the proposed method, the main computational burden is the CAGIF, of which the complexity is $O(N)$ (12). The complexity of the other three methods are also $O(N)$, but with much larger leading constants. Taking the *Anisotropic* method for example, the parameter that controls the diffusion needs to be determined at each iteration, which is the bottleneck of this method. For the *BM3D* method, the leading constant is at least $(2N_gN_s^2)/(N_{\text{step}}^2)$, where N_g is the maximum size of a group, N_s^2 is the size of the search neighborhood for block-matching, and N_{step} is the sliding step (13). In short, a main advantage of the proposed CAGIF method over other the state-of-the-art methods is much faster.

To support this argument, we extract SPN from images of *small* size and *original* size with different methods. Average running time comparison is shown in Table 2. The simulations were performed with Matlab on a computer with a 3.1 GHz Intel CPU and with 4 GB RAM. Taking the *original*-size images for example, the proposed method can save up to 77% running time compared with the *wavelet* method and can save up to 85% running time compared with the *Anisotropic* method. Note for the *BM3D* method, the plain code is not available for us and the complied mex function is used instead. Taking the time-consuming searching and grouping process into consideration, the *BM3D* method without complied mex function is likely much slower than that shown in Table 2.

In the light of the rapid development of graphics processing unit (GPU), the proposed method is also compared with the other state-of-the-art SCI methods on a GPU sever (Nvidia Tesla M2075 with 6 GB graphic memory). The results in Table 3 show that the proposed method is also much faster than other state-of-the-art methods on a GPU. Taking the *original*-size images for example, the proposed method cost only 0.71s to extract the SPN from an image, which saves up to 60% running time compared with the *wavelet* method and 85% running time compared with the *Anisotropic* method. The *BM3D* method is not tested on GPU since its GPU implementation is not available for us.

Conclusion

In this paper, a novel SCI method based on CAGIF was proposed. The newly developed CAGIF is introduced to extract SPN from an image. Compared with other state-of-the-art SCI methods, the proposed method is much faster due to the low complexity of CAGIF. This advantage makes the proposed method particularly suitable for the real-time SCI application. Despite the advantage of speed, extensive experiments also show that the proposed method can achieve comparable or better performance than the state-of-the-art methods in terms of accuracy. In the future, we intend to improve the proposed method based on a better understanding the nature of SPN.

Acknowledgments

The authors thank the authors of ref. (14) for discussing the parameter setting about applying BM3D for SCI purpose.

References

1. Swaminathan A, Wu M, Liu KJR. Component forensics, theory methodologies, and applications. IEEE Signal Process Mag 2009;26(2):38–48.
2. Janesick JR. Scientific charge-coupled devices. Bellingham, WA: SPIE, 2001; Volume PM83.
3. Lukas J, Fridrich J, Goljan M. Digital camera identification from sensor pattern noise. IEEE Trans Inf Forensics Secur 2006;1:205–14.
4. Mihcak MK, Kozintsev I, Ramchandran K. Spatially adaptive statistical modeling of wavelet image coefficients and its application to denoising. 1999 IEEE International Conference of Acoustics, Speech, and Signal Processing; 1999 March 15–19; Phoenix, AZ. Piscataway, NJ: Institute of Electrical and Electronics Engineers, 1999;3253–6.
5. Cortiana A, Conotter V, Boato G, Natale F. Performance comparison of denoising filters for source camera identification. Proceedings of SPIE 7880, Conference on Media Watermarking, Security and Forensics III, 788007; 2011 Jan 23–26; San Francisco, CA. Bellingham, WA: Society of Photo-Optical Instrumentation Engineers (SPIE), 2011;1–6.
6. Van Houten W, Geradts Z. Using anisotropic diffusion for efficient extraction of sensor noise in camera identification. J Forensic Sci 2012;57(2):521–7.
7. Chen M, Fridrich J, Goljan M, Lukas J. Determining image origin and integrity using sensor noise. IEEE Trans Inf Forensics Secur 2008;3 (1):74–90.
8. Goljan M. Digital camera identification from images – estimating false acceptance probability. In: Kim HJ, Katzenbeisser S, Ho ATS, editors. Proceedings of the 7th International Workshop on Digital Watermarking (IWDW 2008); 2008 Nov 10–12; Busan, Korea. Heidelberg, Germany: Springer Berlin Heidelberg 2009;5450:454–68.
9. Tomioka Y, Ito Y, Kitazawa H. Robust digital camera identification based on pairwise magnitude relations of clustered sensor pattern noise. IEEE Trans Inf Forensics Secur 2013;8(12):1986–95.
10. Kang X, Li Y, Qu Z, Huang J. Enhancing source camera identification performance with a camera reference phase sensor pattern noise. IEEE Trans Inf Forensics Secur 2012;7(2):393–402.
11. Li CT. Source camera identification using enhanced sensor pattern noise. IEEE Trans Inf Forensics Secur 2010;5(2):280–7.

12. Li Z, Zheng J, Zhu Z. Content adaptive guided image filtering. 2014 IEEE International Conference on Multimedia and Expo (ICME); 2014 July 14–18; Chengdu, China. Piscataway, NJ: Institute of Electrical and Electronics Engineers, 2014;1–6.
13. Dabov K, Foi A, Katkovnik V, Egiazarian K. Image denoising by sparse 3D transform-domain collaborative filtering. IEEE Trans Image Process 2007;16(8):2080–95.
14. Chierchia G, Parrilli S, Poggi G, Sansone C, Verdoliva L. On the influence of denoising in PRNU based forgery detection. Proceedings of the 2nd ACM Workshop on Multimedia in Forensics, Security and Intelligence; 2010 Oct 25–29; Firenze, Italy. New York, NY: Association for Computing Machinery, 2010;117–22.
15. Perona P, Malik J. Scale-space and edge detection using anisotropic diffusion. IEEE Trans Pattern Anal Mach Intell 1990;12:629–39.
16. He K, Sun J, Tang X. Guided image filtering. IEEE Trans Pattern Anal Mach Intell 2013;35(6):1397–409.
17. Rudin LI, Osher S, Fatemi E. Nonlinear total variation based noise removal algorithms. Physica D 1992;60(1–4):259–68.
18. Gloe T, Bohme R. The Dresden image database for benchmarking digital image forensics. J Digital Forensic Pract 2010;3(2–4):150–9.

Additional information and reprint requests:
Hui Zeng, Ph.D.
School of Information Science & Tech.
Sun Yat-sen University
Guangzhou 510006
China
E-mail: zengh5@mail2.sysu.edu.cn